Collisional absorption of dense plasmas in strong laser fields: Quantum statistical results and simulation

Paul Hilse and Manfred Schlanges
Institut für Physik, Ernst-Moritz-Arndt-Universität Greifswald, D-17489 Greifswald, Germany

Thomas Bornath* and Dietrich Kremp
Institut für Physik, Universität Rostock, D-18051 Rostock, Germany
(Received 22 November 2004; published 31 May 2005)

Collisional absorption of dense fully ionized plasmas in strong laser fields is investigated using quantum statistical methods as well as molecular dynamics simulations. For high-frequency fields, quantum statistical expressions for the electrical current density and the electron-ion collision frequency are presented. Strong correlations are taken into account and their influence on the absorption rate is discussed. The expressions are valid for arbitrary field strength assuming the nonrelativistic case. In addition, molecular dynamics simulations were performed to calculate the heating of dense plasmas in laser fields. Comparisons with the analytic results for different plasma parameters are given. There are considered the cases of isothermal plasmas as well as two-temperature plasmas. Furthermore, results for the velocity distribution function under the influence of intense laser fields are presented which show a different behavior in comparison to weak fields.

DOI: 10.1103/PhysRevE.71.056408 PACS number(s): 52.25.Dg, 05.30.−d

I. INTRODUCTION

An important question in almost all experiments with interaction of intense laser pulses with matter is the calculation of the energy deposition and the description of the heating connected with that. If a solid target is irradiated by such an intense laser pulse, dense plasmas can be created. One of the important mechanisms of energy deposition is inverse bremsstrahlung, i.e., laser light absorption via collisional processes between the plasma particles usually described in terms of the electron-ion collision frequency.

In several papers, various approaches were used to calculate the electron-ion collision frequency and the dynamic conductivity, respectively, for classical plasmas under different conditions [1–6].

Quantum mechanical treatments were given by several authors, e.g., [7–10]. Rigorous quantum kinetic approaches, however, to the inverse bremsstrahlung absorption in dense plasmas were missing until recently. Kremp *et al.* [11] derived a quantum kinetic equation for dense plasmas in strong laser fields using nonequilibrium Green's function techniques. In this approach, the different interaction processes can be taken into account by appropriate approximations of the generalized field-dependent scattering rates including nonlinear field effects such as multiphoton processes and higher-harmonic generation. Time-dependent phenomena were studied by numerical solution of this equation [12,13] in the statically screened Born approximation.

Quantum expressions for the collision term and the electron-ion collision frequency including dynamic screening were given in [14]. A quantum theory based on the dielectric approximation [15] leads to similar results.

Generalizations in order to study effects of strong electron-electron and ion-ion correlations on the collisional absorption rate were given in [16,17] and in [18].

Simulations of inverse bremsstrahlung absorption were performed by Pfalzner and Gibbon [19] who used tree code molecular dynamics enforcing a single temperature for electrons and ions. Collisional electron heating using molecular dynamics was considered also in Ref. [20]. Calculations of heating rates in a classical test particle approach were performed in [21].

The purpose of the present paper is twofold. First, within the analytical approach developed recently, we will give results for the important case of a two-temperature plasma. We will discuss especially the influence of strong coupling effects on collisional absorption. Second, we have performed molecular dynamics simulations without the restriction to a single temperature. Comparison of the simulation data with the analytical results is given.

II. COLLISIONAL ABSORPTION FOR STRONGLY CORRELATED PLASMAS

We want to give here a short summary of the theory we developed elsewhere [14,16,17]. As we are interested here in the collisional absorption by the dense plasma, it is obvious to start from the balance equation for the energy and the electrical current resulting from a generalized non-Markovian kinetic equation. The energy balance reads

$$\frac{dW^{\mathrm{kin}}}{dt} - \mathbf{j}\cdot\mathbf{E} = \sum_{a,b} \int \frac{d^3k_a}{(2\pi\hbar)^3} \frac{k_a^2}{2m_a} I_{ab}(\mathbf{k}_a). \tag{1}$$

It was shown that the right-hand side (RHS) of Eq. (1) with a non-Markovian collision integral gives just the contribution of the mean value of the potential energy [14]. Thus the energy balance (1) is given by

*Electronic address: thomas.bornath@uni-rostock.de

$$\frac{dW^{\mathrm{kin}}}{dt} + \frac{dW^{\mathrm{pot}}}{dt} = \mathbf{j}\cdot\mathbf{E}, \tag{2}$$

where the RHS is in turn the energy loss of the electromagnetic field due to Poynting's theorem.

For the calculation of the collisional absorption, it is appropriate to start from the general balance equation for the current density in the following form:

$$\frac{d}{dt}\mathbf{j}_a(t) - n_a\frac{e_a^2}{m_a}\mathbf{E}(t) = \sum_{b\neq a}\int\frac{d^3q}{(2\pi\hbar)^3}\frac{e_a\mathbf{q}}{m_a}V_{ab}(q)L_{ab}^{<}(\mathbf{q};t,t) \tag{3}$$

where $i\hbar L_{ab}^{<}(t,t') = \langle\delta\rho_b(t')\delta\rho_a(t)\rangle$ denotes the correlation function of the density fluctuations which can be determined within nonequilibrium Green's functions methods from the following general equations of motion:

$$L_{ab} = \Pi_{ab} + \sum_{c,d}\Pi_{ac}V_{cd}L_{db} \tag{4}$$

with Π_{ab} being the so-called polarization function. For the case of no external field one would get in lowest approximation the random phase approximation (RPA).

In a plasma in a strong laser field, the coupling between species with different charges can be considered to be weak, whereas the coupling between particles with equal charges is not affected by the strong laser field. Therefore an approximation in lowest order of V_{ei} seems to be appropriate and the polarization functions Π_{ab} can be adopted to be diagonal, $\Pi_{ab}=\delta_{ab}\Pi_a$. The subsystems, however, may be strongly coupled.

The dependence on the electric field can be made explicit [16,17]. It has an exponential form and causes thus nonlinear effects like multiphoton absorption and the occurrence of higher harmonics in the current. For a harmonic electric field, $\mathbf{E}=\mathbf{E}_0\cos\omega t$, the exponential prefactor can be expanded into a Fourier series. The current balance is given then by

$$\begin{aligned}\frac{d}{dt}\mathbf{j}_e(t) - n_e\frac{e_e^2}{m_e}\mathbf{E}(t) = \mathrm{Re}\int\frac{d^3q}{(2\pi\hbar)^3}\frac{2\pi e_e\mathbf{q}}{m_e\hbar}&\\ \times V_{ei}^2(q)\sum_m\sum_n(-i)^{m+1}J_n\left(\frac{\mathbf{q}\cdot\mathbf{v}_0}{\hbar\omega}\right)&\\ \times J_{n-m}\left(\frac{\mathbf{q}\cdot\mathbf{v}_0}{\hbar\omega}\right)e^{im\omega t}\int_{-\infty}^{\infty}\frac{d\bar{\omega}}{2\pi}[\mathcal{S}_{ee}(\mathbf{q};\bar{\omega}-n\omega)\mathcal{L}_{ii}^{A}(\mathbf{q};\bar{\omega})&\\ + \mathcal{L}_{ee}^{R}(\mathbf{q};\bar{\omega}-n\omega)\mathcal{S}_{ii}(\mathbf{q};\bar{\omega})],&\end{aligned} \tag{5}$$

with the one-component structure factors and response functions $\mathcal{S}_{aa}$ and $\mathcal{L}_{aa}$, respectively [16,17]. We will assume in the rest of this section that the subsystems are in local thermodynamic equilibrium with temperatures T_e and T_i, respectively. J_l is the Bessel function of lth order and $\mathbf{v}_0 = (e_e/m_e)\mathbf{E}_0/\omega$.

In the above equation electron and ion functions contribute equally to the screening. The ion dynamic structure factor $\mathcal{S}_{ii}$ and the response function $\mathcal{L}_{ii}$, however, are localized in the low-frequency region, i.e., for a high-frequency electric field, $\bar{\omega}$ can be neglected in comparison with $n\omega$. In this case, the first term in the brackets in Eq. (5) vanishes because $\int d\bar{\omega}\,\mathcal{L}_{ii}^{A}(\mathbf{q};\bar{\omega})=0$, and for the current it follows that

$$\begin{aligned}\mathbf{j}_e(t) - \int_{-\infty}^{t}d\bar{t}\frac{n_e e_e^2}{m_e}\mathbf{E}(\bar{t}) = \mathrm{Re}\int\frac{d^3q}{(2\pi\hbar)^3}\sum_m\sum_n\frac{e_e}{m_e}\frac{\mathbf{q}}{m\hbar\omega}V_{ei}^2(q)&\\ \times(-i)^{m+2}e^{im\omega t}J_n\left(\frac{\mathbf{q}\cdot\mathbf{v}_0}{\hbar\omega}\right)J_{n-m}\left(\frac{\mathbf{q}\cdot\mathbf{v}_0}{\hbar\omega}\right)\mathcal{L}_{ee}^{R}(\mathbf{q};-n\omega)&\\ \times n_i\mathcal{S}_{ii}(\mathbf{q})&\end{aligned} \tag{6}$$

where screening by the ions is accounted for by the static structure factor $\mathcal{S}_{ii}(\mathbf{q})$ defined by

$$\mathcal{S}_{ii}(\mathbf{q}) \equiv \frac{1}{n_i}\int d\bar{\omega}\,\mathcal{S}_{ii}(\mathbf{q},\bar{\omega}) = 1 + n_i\int d^3r[g_{ii}(\mathbf{r})-1]e^{-(i/\hbar)\mathbf{q}\cdot\mathbf{r}}, \tag{7}$$

where $g_{ii}(r)$ is the pair correlation function.

The Fourier coefficients of the current can be identified easily from Eq. (6). Only the odd harmonics are allowed due to the symmetry of the interaction; cf. [14].

An important quantity is the cycle averaged dissipation of energy $\langle\mathbf{j}\cdot\mathbf{E}\rangle$,

$$\begin{aligned}\langle\mathbf{j}\cdot\mathbf{E}\rangle = n_i\int\frac{d^3q}{(2\pi\hbar)^3}V_{ii}(q)\mathcal{S}_{ii}(\mathbf{q})&\\ \times\sum_{n=-\infty}^{\infty}n\omega\,J_n^2\left(\frac{\mathbf{q}\cdot\mathbf{v}_0}{\hbar\omega}\right)\mathrm{Im}\,\varepsilon_{ee}^{-1}(\mathbf{q};-n\omega),&\end{aligned} \tag{8}$$

with the imaginary part of the dielectric function of the electron subsystem

$$\mathrm{Im}\,\varepsilon_{ee}^{-1}(\mathbf{q};-n\omega) = V_{ee}(q)\mathrm{Im}\,\mathcal{L}_{ee}^{R}(\mathbf{q};-n\omega).$$

Often there is also the electron-ion collision frequency ν_{ei} discussed which is defined for the high-frequency case by (ω_p is the plasma frequency)

$$\nu_{ei} = \frac{\omega^2}{\omega_{\mathrm{p}}^2}\frac{\langle\mathbf{j}\cdot\mathbf{E}\rangle}{\langle\epsilon_0\mathbf{E}^2\rangle}. \tag{9}$$

Equation (8) is a generalization of the theory developed in [14]. Approximating $\mathcal{S}_{ii}(\mathbf{q})\approx 1$ and using $\mathcal{L}_{ee}^{R}$ in the RPA, one gets the results of Sec. IV in that former paper. Now there is included the static stucture factor of the ion component. Further, the function $\mathcal{L}_{ee}^{R}$ is the exact density response function of the electron subsystem, i.e., the electron-electron interaction can be included on a very high level. Appropriate approximations can be expressed via local field corrections (LFCs) (see, e.g., [22,23])

$$\mathcal{L}_{ee}^{R}(\mathbf{q},\omega) = \frac{\chi_e^0(\mathbf{q},\omega)}{1 - V_{ee}(q)G(q)\chi_e^0(\mathbf{q},\omega)} \tag{10}$$

with χ_e^0 being the usual free-electron Lindhard polarizability depending on the local equilibrium electron distribution function.

With Eqs. (8) and (9), we are able to describe the collisional absorption for the case of a two-temperature plasma.

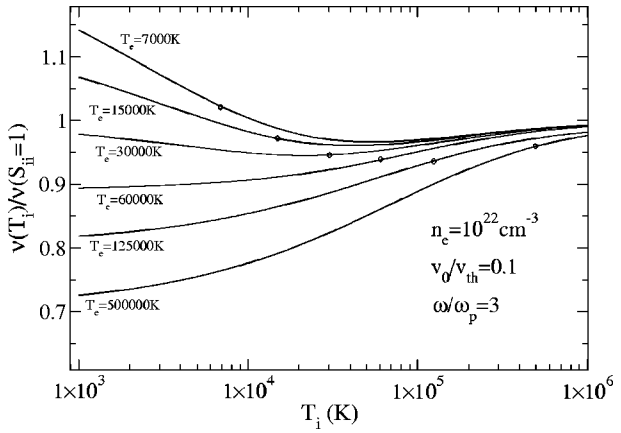

FIG. 1. Ratio of collision frequencies with the structure factor in HNC approximation to values with $\mathcal{S}_{ii}=1$ as a function of the ion temperature T_i. There are shown curves for different electron temperatures T_e; as a guide for the eye, the circles mark the case of an isothermal plasma where $T_e=T_i$.

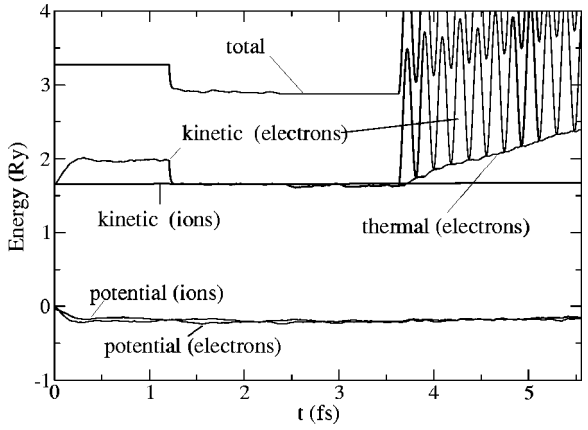

FIG. 2. Time evolution of the particle energies of a hydrogen plasma at the beginning of the simulation. The parameters are field strength $E_0=2.85\times10^9$ V/cm corresponding to an intensity $I=10^{16}$ W/cm^2; electron density $n_e=10^{22}$ cm^{-3}; laser frequency $\omega/\omega_p=3$.

As we will see later, also molecular dynamics (MD) simulations confirm that mainly the electrons are heated by the laser field whereas the temperature of the ions stays almost constant. The influence of the ion component with temperature T_i is accounted for in Eq. (8) by the static ionic structure factor. There we adopted an already fully ionized plasma under the influence of a laser. Results are shown in Fig. 1 for an ion structure factor in the hypernetted chain (HNC) approximation. The calculations show a considerable influence of structure factor effects on collisional absorption especially for the case $T_i<T_e$. Only for comparatively small electron temperatures is there an enhancement of the collision frequency at all. For high electron temperatures and $T_i\ll T_e$, the inclusion of the ion structure factor can reduce the collision frequency by about 25%.

As was pointed out by Langdon [24], for strong fields the electron-electron collisions may not be efficient enough to establish a Maxwellian distribution. This behavior can be described by a so-called super-Maxwellian distribution [25]

$$f_m(v) = C_m \exp\left[-\left(\frac{v}{v_m}\right)^m\right], \tag{11}$$

with

$$C_m = \frac{m}{4\pi\Gamma(3/m)v_m^3},$$

$$m(\alpha) = 2 + 3/(1 + 1.66/\alpha^{0.724}), \quad \alpha = Zv_0/v_{\rm th},$$

$$v_{\rm th}^2 = 1/3 \int d^3v\, v^2 f(v),$$

$$v_m^2 = \frac{3\Gamma(3/m)}{\Gamma(5/m)} v_{\rm th}^2.$$

Below we will present also results of calculations [26] with such a distribution function instead of a Maxwellian.

III. MOLECULAR DYNAMICS SIMULATIONS

In an alternative approach we calculated the energy absorption with molecular dynamics simulations. The main difficulty in order to simulate a fully ionized plasma is to model the attractive electron-ion interaction: the pure Coulomb potential has a singularity at the origin which causes a nonphysical behavior of the system. To avoid this divergence and to include quantum effects, we used the Kelbg potential [27] which is given by

$$\Phi_{ij} = \frac{q_i q_j}{4\pi\epsilon_0 r}\{1 - \exp(-r^2/\lambda_{ij}^2) + \sqrt{\pi} r/\lambda_{ij}[1 - \mathrm{erf}(r/\lambda_{ij})]\}. \tag{12}$$

This potential has a finite value at the origin, and it is temperature dependent via the thermal wavelength $\lambda_{ij} = \hbar/\sqrt{2\mu_{ij}k_BT}$, where $\mu_{ij}=m_im_j/(m_i+m_j)$ denotes the reduced mass of two particles of species i and j.

The external electric field was implemented as a homogeneous linearly polarized harmonic field. The temperature of the species a was defined as

$$\frac{3}{2}k_BT_a = E_{\rm therm} = m_a\frac{\langle v_a^2\rangle - \langle v_a\rangle^2}{2}, \tag{13}$$

where the angular brackets denote an averaging over all particles of species a. This definition takes into account the undirected motion only. The MD calculations were performed using periodic boundary conditions with Ewald summation [28]. The number of particles was between 2000 and 5000. Figure 2 shows the scenario of the simulation. Kinetic and potential energies of electrons and ions as well as the total energy are given as functions of time. At the start of the simulation, the electrons and ions have the same mean kinetic energy. The first stage of the simulation, up to 0.5 fs, is the so-called establishment of correlations [11] which shows up in a decrease of the potential energy. Because of energy conservation there is a fast increase of the kinetic energy of the electrons. Due to the mass ratio of electrons and ions, the

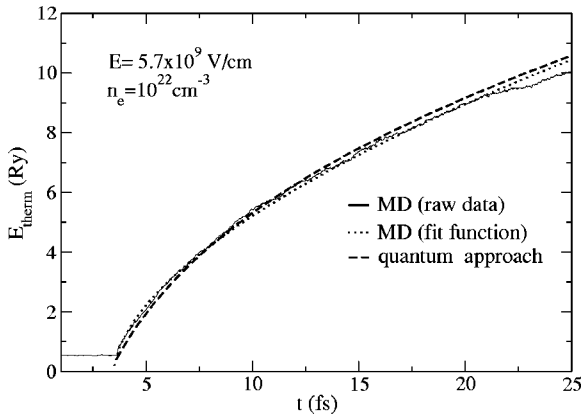

FIG. 3. Time dependence of the thermal energy of the electrons in a hydrogen plasma under the influence of a strong laser field. Laser frequency and intensity are $\omega/\omega_p=3$ and $I=4.3\times10^{16}$ W/cm^2.

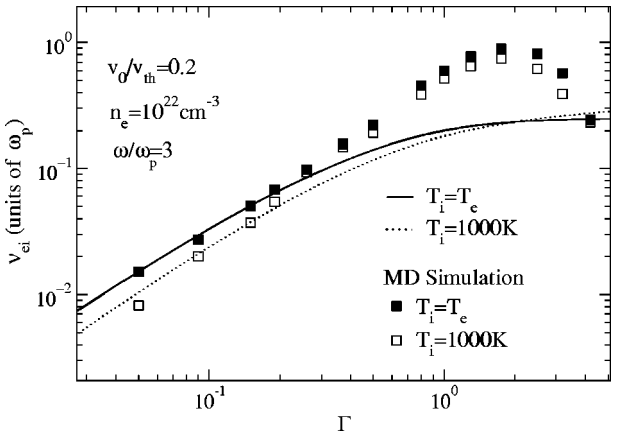

FIG. 4. Electron-ion collision frequency as a function of the coupling parameter $\Gamma=(Ze^2/k_BT_e)[(4\pi/3)n]^{1/3}$ for a hydrogen plasma in a laser field. Solid line, quantum statistical approach for an isothermal plasma ($T_i=T_e$). Dotted line, same approach but for a two-temperature plasma ($T_i=1000$ K). The filled and open squares denote the corresponding simulation data.

system cannot relax to an equilibrium state in the following femtosecond, and a two-temperature plasma is produced.

To start with a defined equilibrium state, the system is thermalized for about 1 fs, t between 1.25 and 2.25 fs. This is done by rescaling the velocities of the particles to get the desired value of the mean kinetic energy. The rescaling corresponds to a coupling to an external heat bath. Of course, in this stage the total energy is not constant. In the next period, t between 2.25 and 3.5 fs, the heat bath is switched off and again the total energy is conserved. Aside from small fluctuations, kinetic as well as potential energies are constant then. Now a defined stable state is reached.

At $t=3.5$ fs the laser is switched on. The kinetic energy of the electrons oscillates with double the laser frequency because the electrons move nearly collectively in a directed motion driven by the external field. Due to the collisions with the ions, a fraction of the gained directed kinetic energy dissipates in random directions and the electrons are heated (increasing of thermal energy). The transfer of energy to ions is quite small, thus their temperature remains nearly constant and again a two-temperature plasma is formed.

The further development of the system is shown in Fig. 3 where the thermal energy of the electrons is plotted. The raw data (solid) show a steady increase of the temperature. The change of thermal energy is associated with the electron-ion collision frequency for the high-frequency case via

$$\nu_{ei}(\omega)=\frac{\omega^2}{\omega_p^2}\frac{2}{\epsilon_0 E_0^2}\frac{dE_{\text{therm}}}{dt}. \tag{14}$$

Thus the determination of heating rates and collision frequencies, respectively, from the simulation data requires the time derivative of the thermal energy. The raw data, however, are very noisy, and that makes a direct numerical derivation impossible. Instead, a fit of the form $E_{\text{therm}}=A(t-C)^B$ was used to get a smooth function for the thermal energy (dotted line in Fig. 3). Keeping in mind $E_{\text{therm}}\equiv 3/2k_BT_e$, one can extract now the collision frequency as a function of the electron temperature. One can see in Fig. 3 that, for a constant field strength, the energy input decreases in the region of high temperatures.

For comparison, results from the quantum kinetic approach are shown (dashed line). The agreement with the quantum kinetic approach which was obtained by time integration of Eq. (14) is very good for the parameters used in this example. There exist, however, also parameter ranges with larger deviations (cf. Fig. 4).

In Fig. 4, the collision frequency normalized to the plasma frequency is plotted as a function of the coupling parameter Γ. The solid and dotted lines are results obtained from Eqs. (8) and (9). The solid line denotes the isothermal case with $T_i=T_e$, whereas the dotted line is the result for a two-temperature plasma with an ion temperature of 1000 K.

The open squares are the corresponding simulation data for the two-temperature plasma. In addition, simulations were performed in which the temperature of the ions was forced to be the same as that of the electrons (filled squares). The simulation data as well as the analytic calculation show an increase of the collision frequency with increasing coupling. The agreement between the simulation and the quantum statistical results is good in the region of weak and moderate coupling (about $\Gamma=0.3$). For small field strengths (about $v_0/v_{\text{th}}\leqslant 0.2$), the slope of the analytic curves is determined by the temperature only, whereas for higher field strengths, there is also a dependence on the oscillatory velocity v_0. The lowering of the collision frequency for a two-temperature plasma with cold ions is very well confirmed by the MD simulations. Physically, this lowering is caused by screening due to the ions.

In the region of higher coupling, $\Gamma>0.3$, the deviations between the simulation and the analytic calculations are growing. Both approaches have their limitations in this region. One has to keep in mind that, on one hand, the analytic approach adopts weak coupling with respect to the electron-ion interaction. On the other hand, molecular dynamics simulations are valid for arbitrary coupling only in the classical case. Quantum effects are accounted for here only ap-

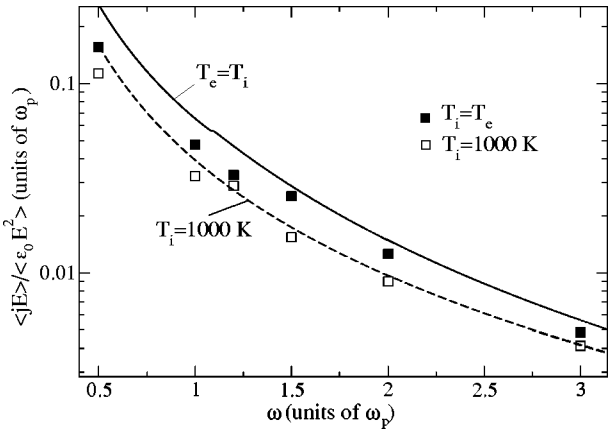

FIG. 5. Energy absorption rate as a function of the laser frequency for a hydrogen plasma in the laser field. The lines denote the analytic result for an isothermal (solid, $T_i=T_e$) and a two-temperature (dashed, $T_i=1000$ K) plasma. The filled and open squares denote the corresponding simulation data ($\Gamma=0.15$, $T_e=33$ eV, $v_0/v_{\text{th}}=0.2$, $n_e=10^{22}$ cm^{-3}).

proximately: the effective quantum potential used in the molecular dynamics has been derived by Kelbg for weakly coupled plasmas only [27].

A further quantity influencing the plasma heating is the laser frequency. Figure 5 shows the energy absorption rate of a hydrogen plasma for different laser frequencies. There are given the results of the analytic approach for isothermal (solid line) and a two-temperature plasma (dashed line), respectively. The filled and open squares are the corresponding simulation data. The heating rate depends strongly on the frequency. With increasing frequency the rate decreases very fast. This behavior of the analytic result is found also in the simulation. The corresponding curve for the collision frequency ν_{ei} has some more structures (see Fig. 8 in [14]), especially for frequencies below ω_p; the collision frequency is almost constant and drops afterward.

Again, the simulations confirm the lowering of the absorption rate for a two-temperature plasma with cold ions.

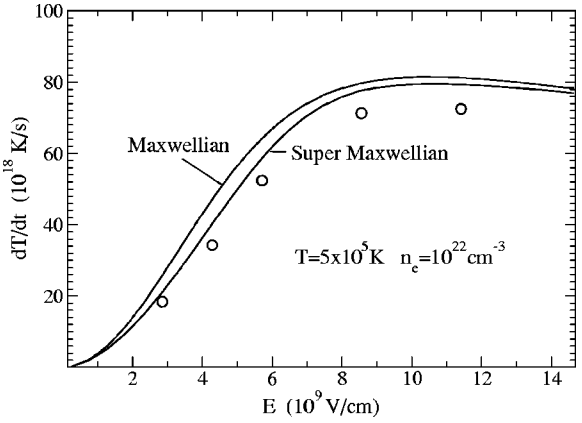

FIG. 6. Heating rate of the electrons in a two-temperature hydrogen plasma ($T_i=1000$ K) as a function of the applied field strength ($\omega/\omega_p=3$). The solid lines denote the analytic results for two different assumptions for the velocity distribution functions. The circles are MD results.

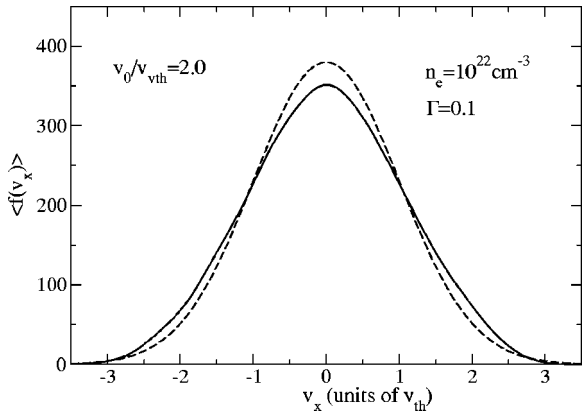

FIG. 7. Velocity distribution function of the electrons (in the field direction) under the influence of an intense laser field. The solid line denotes the simulation data for a field strength of $E=5.7$ GV/cm. For comparison the Maxwell distribution (dashed) is plotted.

For rather high frequencies, the agreement between the simulations and the analytic results is quite good. In the low-frequency regime the deviations are bigger. This, of course, is due to the limitation of our analytic approach to high frequencies whereas the MD simulations have no restriction regarding the frequency.

So far, results were presented for rather small field strength. The analytic model has—in addition to the restriction to the nonrelativistic case—no limitation on the strength of the field. Thus we can compare the analytic theory with simulations even for the strong field regime. Figure 6 shows the heating of the electrons as a function of the applied field strength. The circles denote the simulation data of the corresponding two-temperature plasma where the ion temperature was 1000 K. The solid lines denote results from the analytic approach for a two-temperature plasma. The velocity distribution of the electrons does not remain Maxwellian under the influence of a laser field (cf. the so-called Langdon effect [24]). That is why calculations were performed with different

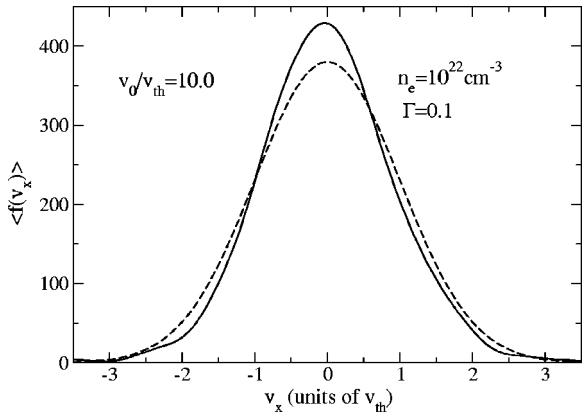

FIG. 8. Velocity distribution function of the electrons (in the field direction) under the influence of an intense laser field. The solid line denotes the simulation data for a field strength of $E=28.5$ GV/cm. For comparison the Maxwell distribution (dashed) is plotted.

assumptions for the velocity distribution function: we considered Maxwellian as well as super-Maxwellian distribution functions (11). There is a better agreement with the simulation data in the case of the super-Maxwellian.

In order to investigate this issue in more detail, the velocity distribution function was determined from simulations for different field strengths. Figure 7 shows the velocity distribution in the direction of the linearly polarized strong laser field for a weakly coupled hydrogen plasma. The solid line denotes the result which was obtained from the simulation with a field strength of 5.7 GV/cm ($v_0/v_{\mathrm{th}}=2$). For comparison the corresponding Maxwell distribution is plotted. One can see that the field leads to a broadening of the distribution function. This is in accordance with results of Pfalzner and Gibbon [19] who considered distribution functions for field strengths up to $v_0/v_{\mathrm{th}}=1$. If the field strength increases further, a different behavior occurs. Figure 8 shows the velocity distribution functions in a laser field where the field strength is 28.5 GV/cm ($v_0/v_{\mathrm{th}}=10$). It can be observed that the distribution function is narrowed. This narrowing is in contrast to the Langdon effect, and it is not a kinematic effect. This was proved by switching off the electron-ion collisions in the simulations. For this case, the distribution functions remain Maxwellian for all field strengths. To our knowledge, such a behavior has not been reported yet. We have, however, no simple physical interpretation for that.

IV. CONCLUSION

We have presented analytical as well as simulation results on collisional absorption focusing especially on the case of a two-temperature plasma. Both approaches show a dependence of the energy absorption not only on the electron temperature but also on the temperature of the heavy ion component. Both temperatures can differ from each other considerably in certain experimental situations. Therefore it is important to take this issue into account, for instance, in hydrodynamic simulations where, so far, often simple Drude models are used.

[1] J. M. Dawson and C. Oberman, Phys. Fluids **6**, 394 (1963).
[2] C. D. Decker, W. B. Mori, J. M. Dawson, and T. Katsouleas, Phys. Plasmas **1**, 4043 (1994).
[3] V. P. Silin, Zh. Eksp. Teor. Fiz. **47**, 2254 (1964) [Sov. Phys. JETP **20**, 1510 (1965)].
[4] P. J. Catto and Th. Speciale, Phys. Fluids **20**, 167 (1977).
[5] Yu. L. Klimontovich, *Kinetic Theory of Nonideal Gases and Nonideal Plasmas* (Nauka, Moscow, 1975) (in Russian) [Pergamon, Oxford, 1982 (in English)].
[6] P. Mulser, F. Cornolti, E. Bésuelle, and R. Schneider, Phys. Rev. E **63**, 016406 (2001).
[7] N. M. Kroll and K. M. Watson, Phys. Rev. A **8**, 804 (1973).
[8] L. Schlessinger and J. Wright, Phys. Rev. A **20**, 1934 (1979).
[9] V. P. Silin and S. A. Uryupin, Zh. Eksp. Teor. Fiz. **81**, 910 (1981) [Sov. Phys. JETP **54**, 485 (1981)].
[10] R. Cauble and W. Rozmus, Phys. Fluids **28**, 3387 (1985).
[11] D. Kremp, Th. Bornath, M. Bonitz, and M. Schlanges, Phys. Rev. E **60**, 4725 (1999).
[12] D. Kremp, Th. Bornath, P. Hilse, H. Haberland, M. Schlanges, and M. Bonitz, Contrib. Plasma Phys. **41**, 259 (2001).
[13] H. Haberland, M. Bonitz, and D. Kremp, Phys. Rev. E **64**, 026405 (2001).
[14] Th. Bornath, M. Schlanges, P. Hilse, and D. Kremp, Phys. Rev. E **64**, 026414 (2001).
[15] H.-J. Kull and L. Plagne, Phys. Plasmas **8**, 5244 (2001).
[16] Th. Bornath, M. Schlanges, P. Hilse, and D. Kremp, J. Phys. A **36**, 5941 (2003).
[17] Th. Bornath, M. Schlanges, P. Hilse, and D. Kremp, in *Nonequilibrium Physics at Short Time Scales: Formation of Correlations*, edited by K. Morawetz (Springer-Verlag, Berlin, 2004), pp. 153–172.
[18] G. Hazak, N. Metzler, M. Klapisch, and J. Gardner, Phys. Plasmas **9**, 345 (2002).
[19] S. Pfalzner and P. Gibbon, Phys. Rev. E **57**, 4698 (1998).
[20] S. A. Maĭorov, Plasma Phys. Rep. **27**, 311 (2001).
[21] A. Brantov *et al.*, Phys. Plasmas **10**, 3385 (2003).
[22] J. Hubbard, Proc. R. Soc. London, Ser. A **243**, 336 (1957).
[23] S. Ichimaru and K. Utsumi, Phys. Rev. B **24**, 7385 (1981).
[24] A. B. Langdon, Phys. Rev. Lett. **44**, 575 (1980).
[25] P. Alaterre, J.-P. Matte, and M. Lamoureux, Phys. Rev. A **34**, 1578 (1986).
[26] M. Schlanges, P. Hilse, Th. Bornath, and D. Kremp, in *Progress in Nonequilibrium Green's Functions*, edited by M. Bonitz and D. Semkat (World Scientific, Singapore, 2003), pp. 50–65.
[27] G. Kelbg, Ann. Phys. **12**, 219 (1963); **13**, 354 (1964); **14**, 394 (1964).
[28] P. P. Ewald, Ann. Phys. **64**, 253 (1921).